

THE PCS OUTLYINGNESS INDEX

BY KAVEH VAKILI*, ERIC SCHMITT*

*KU Leuven**

The Projection Congruent Subset (PCS) Outlyingness is a new index of multivariate outlyingness obtained by considering univariate projections of the data. Like many other outlier detection procedures, PCS searches for a subset which minimizes a criterion. The difference is that the new criterion was designed to be insensitive to the outliers. PCS is supported by FastPCS, a fast and affine equivariant algorithm which we also detail. Both an extensive simulation study and a real data application from the field of engineering show that FastPCS performs better than its competitors.

1. Introduction. Outliers are observations that do not follow the pattern of the majority of the data (Rousseeuw and van Zomeren 1990). Outlier identification is a major part of data analysis for at least two reasons. First, because a few atypical observations can severely influence the results of most procedures and we generally do not want our inferences to depend on them. In addition, we may want to find discordant data points to study them as objects of interest in their own right. In any case, detecting outliers in more than two dimensions is difficult because we can not inspect the data visually and have to rely on algorithms instead.

Formally, this paper concerns itself with the simplest, most basic variant of the multivariate outlier detection problem. The general setting is that of a sample of n observations $x_i \in \mathbf{R}^p$ (with $n > p$), at least $h = \lceil (n+p+1)/2 \rceil$ of which are drawn from a model \mathcal{F} with continuous support. The objective is to identify reliably the index of the remaining ones. A more complete treatment of this topic can be found in the book by Maronna, Martin and Yohai (2006).

In this article we introduce PCS, a new procedure for finding multivariate outliers. We also detail FastPCS, a fast algorithm for computing it. The main output of FastPCS is an outlyingness index measuring how much each observation departs from the pattern set by the majority of the data. The PCS outlyingness index is affine equivariant (meaning that the outlyingness ranking of the observations is not affected by a linear transformation of the data) and can be computed efficiently for moderate values of p and large

Keywords and phrases: Outlier detection, multivariate statistics, computational statistics

values of n .

To derive this index, FastPCS proceeds in two steps. First, it strives to select among many possible h subsets of observations one devoid of outliers. Then, the outlyingness index is simply the distance of each observation to this subset.

For easier outlier detection problems, we find that our approach produces results similar to state of the art outlier detection algorithms. When considering more difficult cases however we find that the solution we propose leads to significantly better outcomes.

In the next section we motivate and define the PCS outlyingness and FastPCS. Then, in Section 3 we compare FastPCS to several competitors on synthetic data. In Section 4 we conduct a real data comparison. In Section 5, we offer closing thoughts and discuss directions for further research.

2. The PCS outlyingness.

2.1. *Motivation.* Throughout this note, we will denote as H_m a subset of the indexes $\{1, 2, \dots, n\}$, of size h . For any H_m we denote its mean and covariance matrix as

$$(2.1) \quad (t_m, S_m) = \left(\text{ave}_{i \in H_m} x_i, \text{cov}_{i \in H_m} x_i \right)$$

and we will write the squared Mahalanobis distance of an observation x_i as

$$(2.2) \quad d_{M,i}^2(t_m, S_m) = (x_i - t_m)' S_m^{-1} (x_i - t_m) .$$

FastPCS starts by selecting among many such subsets an h -subset of observation that minimizes a criterion. Other affine equivariant outlier detection algorithms that proceed in this way are the FastMVE (Maronna, Martin and Yohai 2006), the FastMCD (Rousseeuw and Van Driessen 1999) and the SDE (Stahel 1981). For all four procedures we will denote the chosen h -subset as H_* .

Each of these algorithms relies on a different criterion to select the optimal h -subset. In all cases, there is a straightforward relationship between H_* and the resulting outlyingness index. For example, for FastMVE and FastMCD the outlyingness index is the vector of distances $d_{M,i}^2(t_*, S_*)$. For SDE the outlyingness index is the vector of values of $P_M(x_i)$

$$(2.3) \quad P_M(x_i) = \sup_{a_m \in B_M} \frac{|x_i' a_m - \text{med}_{j=1}^n(x_j' a_m)|}{\text{mad}_{j=1}^n(x_j' a_m)}$$

where B_M is a set of M_p directions orthogonal to hyperplanes spanned by a p -subset of $\{1 : n\}$ and H_* contains the observations with smallest values of $P_M(x_i)$.

In all cases, if H_* itself is contaminated, then the resulting outlyingness index can no longer be depended upon to find the outliers. For FastMVE and FastMCD, H_* is the subset of h observations with smallest covariance matrix determinant and enclosed by the ellipsoid with smallest volume, respectively. Given enough outliers, an adversary can easily confound these two characterizations (for example, by placing outliers on a subspace of \mathbf{R}^p) and ensure that a contaminated h -subset will always be chosen over h -subsets formed of genuine observations.

It is not always recognized that the SDE outlyingness index is also sensitive to the outliers. Given enough outliers, they can always be placed in such a way that the denominator in equation (2.3) will be smaller for some direction a_* along which the numerator is smaller for outliers than for genuine observations (for example, consider a direction a_* close to the principal axis of the orange ellipse in the lower-left panel in Figure 1). Then, for many observations the maximum outlyingness will be attained at $a_m = a_*$. Repeated over a large number of such directions, this will cause the value of the outlyingness index in equation (2.3) to be smaller for many outliers than for genuine observations.

Consider the following example. The four panels in Figure 1 all depict the same 70 draws from a standard bivariate normal distribution together with 30 draws from a second normal distribution with smaller variance and centered at $(5, -1)$. Orange ellipses in the first three plots show the (t_*, S_*) obtained using the best subset found by the FastMCD, FastMVE and SDE. These were computed with the R package `rrcov` (Todorov and Filzmoser 2009), using default settings; 500 starting p -subsets (for the first two), and 500 directions a_m (for SDE); and 50 percent BDP in all cases.

In all three cases, the fitted ellipses (drawn in solid orange lines), fail to adequately fit any h -subset of the data, including the subset they enclose. In particular, their centers of symmetry (orange stars) are not located in areas of highly concentrated observations. In all cases, the model fitted on H_* appears visually distinct from the distribution governing the good part of the data (drawn as a dashed blue ellipse). This is confirmed by the biases (a dimensionless measure of dissimilarity between two subsets, see Section 3) of 7, 5 and 3.5 for the three algorithms.

The algorithm we propose differs from these methods in that it uses a new measure of multivariate congruence (which we detail in the next section) to select the optimal h -subset. The main advantage of this new characterization

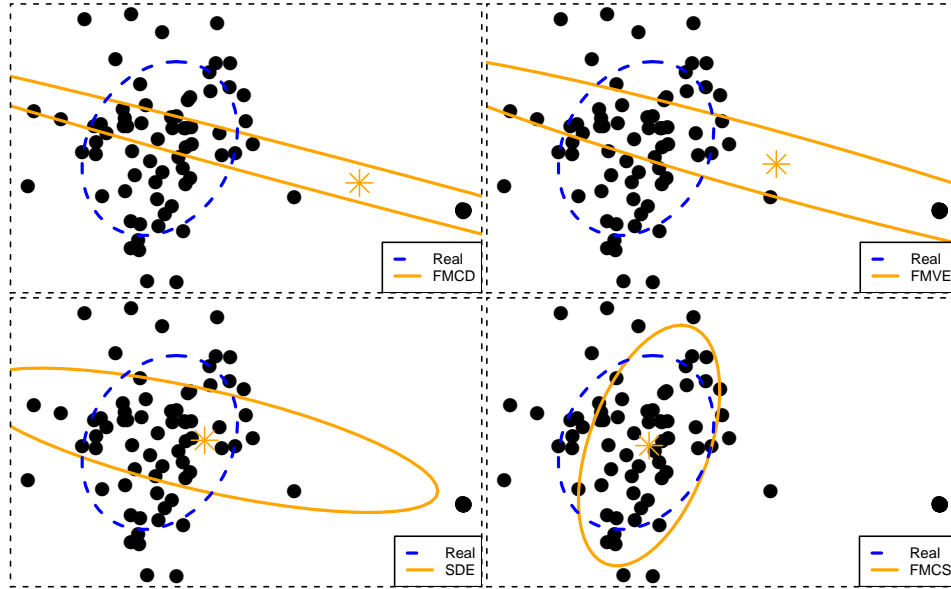


FIG 1. The four plots depict (left right, top, bottom) the same configuration of observations. The blue dashed ellipses show the contours of the model governing the distribution of the majority –here 70 out of 100– of the observations. The orange ellipses show, respectively, the FastMCD, FastMVE, SDE and FastPCS estimates of scatter and location.

lies in its insensitivity to the outliers. As we argue below, this makes the outlyingness index derived from FastPCS both quantitatively and qualitatively more reliable.

2.2. Construction of the PCS Outlyingness. PCS looks for the h -subset of multivariate observations that is most *congruent* along many univariate projections. In this context, we measure the congruence of a given h -subset along a given projection by the size of its overlap with a second subset that is optimal (in a sense we make precise below) on that projection.

In essence, for a given initial h -subset and a random univariate projection we find a second h -subset that minimizes a criterion on that projection and measure the size of the overlap of the two subsets. The PCS criterion is based on the observation that a spatially cohesive h -subset will tend to be congruent with these optimal h -subsets, and a spatially disjoint one will not.

More precisely, for a given p -vector a_{mk} , $d_{P,i}$ will denote the orthogonal distances of the x_i 's to a_{mk} :

$$(2.4) \quad d_{P,i}^2(a_{mk}) = (x_i' a_{mk} - 1)^2.$$

The set of h observations with smallest $d_{P,i}^2(a_{mk})$ will be denoted as H_{mk} . For a given subset H_m and direction a_{mk} we define the *incongruence index*

of H_m along a_{mk} as

$$(2.5) \quad I(H_m, a_{mk}) := \log \frac{\text{ave}_{i \in H_m} d_{P,i}^2(a_{mk})}{\text{ave}_{i \in H_{mk}} d_{P,i}^2(a_{mk})}.$$

This index is always positive and will have small value if the projection of the members of H_m along a_{mk} greatly overlap with the members of H_{mk} . To remove the dependence of equation (2.5) on a_{mk} we measure the incongruence of H_m considering the average over many directions:

$$(2.6) \quad I(H_m) := \text{ave}_{a_{mk} \in B(H_m)} I(H_m, a_{mk})$$

where $B(H_m)$ are all directions orthogonal to a hyperplane spanned by a p -subset of H_m . We call the H_m with smallest $I(H_m)$ the *projection congruent subset*. In essence, The I index measures the incongruence of an h -subset H_m in terms of how much the projection of its members overlap with those of the H_{mk} over many projections. In practice, it would be infeasible to evaluate equation (2.6) over all members of $B(H_m)$. A practical solution is to take the average over a sample of K random directions $\tilde{B}_K(H_m)$.

The I index of a spatially disjoint h -subset tends to be higher than that of a spatially cohesive h -subset. This is because when H_m forms a spatially cohesive set of observations, $|\{H_m \cup H_{mk}\}|$ tends to be larger.

This is illustrated on an example in Figure 2. Both panels depict the same set of $n = 100$ points. These points form two disjoint groups of observations. The main group contains 70 points and is located on the left hand side. Each panel illustrates the behavior of the I index for a given h -subset of observations. H_1 (left) forms a set of spatially cohesive observations, all belonging to the main group. H_2 , in contrast, forms a spatially disjoint set of observations and contains members drawn from both groups. For each H_m -subset, $m = \{1, 2\}$, we drew two hyperplanes a_{m1} (blue, dashed) and a_{m2} (orange). The blue dots show the members of $\{H_m \cup \{H_{m1}\}\}$. Similarly, the cockade dots (orange inside, blue outside) show the members of $\{H_m \cup H_{m2}\}$. The black diamonds show the members of H_{m1} (H_{m2}) that do not belong to H_m . After just two projections, the number of non-overlapping observations (i.e. $\{H_m \setminus H_{m1}\} \cap \{H_m \setminus H_{m2}\}$) is 8 ($m = 1$) and 18 ($m = 2$) respectively. As we increase the number of directions a_{mk} , this pattern repeats and the difference between a spatially cohesive and a disjoint subset grows steadily.

The I index measures the size of this overlap. For a direction a_{mk} , the members of H_{m1} and H_{m2} not in H_m (shown as black square and diamonds in Figure 2) will decrease the denominator in equation (2.5) without affecting

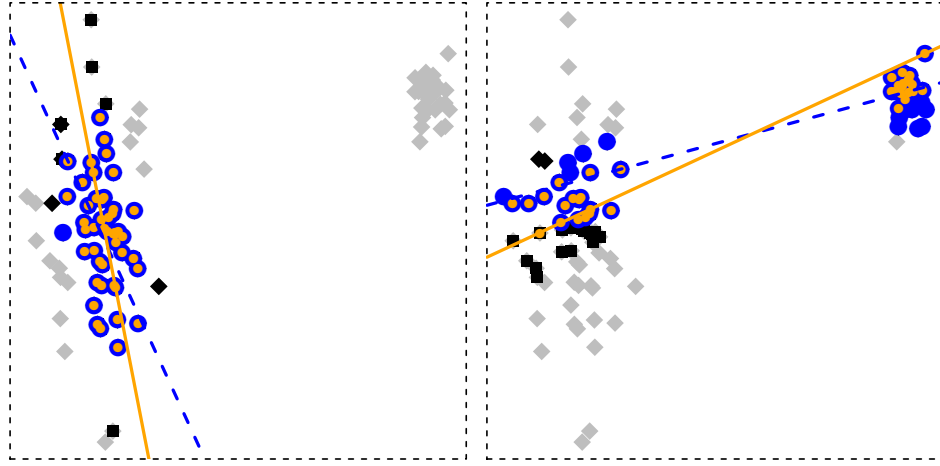


FIG 2. *Incongruence index for a subset H_1 of spatially cohesive observations (left) and a subset H_2 of spatially disjoint observation (right).*

the numerator, increasing the overall ratio. Consequently, h -subsets formed of spatially disjoint groups of observations will have larger values of the I index. Crucially, the I index characterizes a cohesive h -subset of observations independently of the spatial configuration of the outliers. For example, the pattern shown in Figure 2 would still hold if the cluster of outliers were more spatially concentrated. This is also illustrated in the fourth quadrant of Figure 1 where the optimal h -subset found by FastPCS is not unduly attracted by members of the smaller cluster of concentrated observations located on the right.

In Sections 3 and 4, we show that this new characterization allows FastPCS to reliably select uncontaminated h -subsets. This includes many situations where other algorithms fail to do so. First though, the following section details the FastPCS algorithm.

2.3. A Fast Algorithm for the PCS Outlyingness. To compute the PCS outlyingness index, we propose the FastPCS algorithm (2.7). It combines ideas from FastMCD (the use of random p -subsets as starting points and an iterative concentration step) with some new ones. Throughout, M_p denotes the number of starting p subsets.

Our algorithm can detect exact fit situations (when h or more observations lie on an hyperplane). When at least h points lie in an exact fit, FastPCS will return the index of those h observations. In real datasets, exact fits are rare. Nevertheless, handling them is important also for theoretical reason (Rousseeuw 1994).

The second branch of the algorithm starts at b . Step b grows the size of

H_m from h_0 to its final size $h = \lceil (n + p + 1)/2 \rceil$ in L steps, rather than in one as is done in FastMCD. This improves the robustness of the algorithm when outliers are close to the good data. We find that increasing L does not improve performance much if L is greater than 3 and use $L = 3$ as default.

(2.7) Algorithm FastPCS

for $m = 1$ to M_p do:

a: $H_m \leftarrow \{p + 1 \text{ observations drawn at random from } 1 : n\}$

$h_0 \leftarrow$ the smallest integer for which $\binom{h_0}{p} \geq K$

set $H_m \leftarrow \{i : d_{M,i}^2(t_m, S_m) \leq d_{M,(h_0)}^2(t_m, S_m)\}$

b: for $l = 1$ to L do:

$$D_i(H_m) \leftarrow \frac{K}{\text{ave}_{k=1}^K \frac{d_{P,i}^2(a_{mk})}{\text{ave}_{j \in H_m} d_{P,j}^2(a_{mk})}} \quad \text{for all } i = 1, \dots, n$$

set $h_l \leftarrow \lceil (n - p - 1)l / (2L) \rceil + p + 1$

set $H_m \leftarrow \{i : D_i(H_m) \leq D_{(h_l)}(H_m)\}$ ('concentration step')

end for

c: compute $I(H_m) \leftarrow \frac{K}{\text{ave}_{k=1}^K I(H_m, a_{mk})}$

end for

Keep H_* , the subset H_m with lowest $I(H_m)$. The outlyingness index of each observation is given by $D_i(H_*)$.

Empirically also, we found that small values for K are sufficient to achieve good results and that we do not gain much by increasing K above 25, so we set $K = 25$ as the default. That such a small number of random directions suffice to reliably identify the outliers is remarkable. This is because FastPCS uses directions generated by p -subsets of H_m .

Compare this to SDE algorithm which needs a much larger number of projections to reliably find the outliers. This is because in SDE the data is projected along directions given by hyperplanes passing by p points drawn indiscriminately from the entire set of observations. Consequently, when the contamination rate is high, most of these p -subsets will be contaminated, yielding directions that can end up almost parallel to each other. In contrast, our choice always ensures a wider spread of directions when H_m is uncontaminated and thus yields better results.

Like FastMCD and FastMVE, FastPCS uses many random p subsets as starting points. The number of initial p -subsets, M_p , must be large enough to ensure that at least one of them is uncontaminated. For each starting p -subset, the time complexity of these algorithms scales as $O(p^3 + np^2)$. The

random directions used in the SDE are orthogonal to hyperplanes passing by p -points. Here also, the number of such hyperplanes must be of order M_p to ensure that at least one of them does not pass by any of the outliers.

The value of M_p grows exponentially with p . In practice this means all four procedures become impractical for values of p much larger than 25. All four procedures belong to the class of so called ‘embarrassingly parallel’ algorithms, i.e. their time complexity scales as the inverse of the number of processors meaning that they are particularly well suited to benefit from modern computing environments. To enhance user experience, we implemented FastPCS in C++ code wrapped in a portable R package (R Development Core Team, 2012).

3. Empirical Comparison: Simulation Study. In this section we evaluate FastPCS numerically and contrast its performance to that of the SDE, FastMCD and FastMVE algorithms. The last three were computed using the R package `rrcov` with default settings (except, respectively, for the number of random directions and starting subsets which for all algorithms we set according to equation (3.5)). Each algorithm returns a subset H_* of h observations with smallest outlyingness index. Our evaluation criteria are the bias and the misclassification rate of these h observations. Below, we briefly describe these.

3.1. Asymptotic Bias. Given a central model \mathcal{F}_u an arbitrary distribution \mathcal{F}_c , consider a contamination model

$$(3.1) \quad \mathcal{F}_\varepsilon = (1 - \varepsilon)\mathcal{F}_u(\mu_u, \Sigma_u) + \varepsilon\mathcal{F}_c(\mu_c, \Sigma_c) .$$

For a subset of observations H_* , the (asymptotic) bias measures the deviation of (t_*, S_*) from the true (μ_u, Σ_u) . Formally, denoting $G = |S|^{-1/p}S$ and $\Gamma = |\Sigma|^{-1/p}\Sigma$, we have that for an affine equivariant scatter matrix S , all the information about the bias is contained in the matrix $G^{-1/2}\Gamma G^{-1/2}$ or equivalently its condition number (Yohai and Maronna 1990):

$$(3.2) \quad \text{bias}(S) = \log \frac{\lambda_1(G^{-1/2}\Gamma G^{-1/2})}{\lambda_p(G^{-1/2}\Gamma G^{-1/2})}$$

where λ_1 (λ_p) are the largest (smallest) eigenvalues of $G^{-1/2}\Gamma G^{-1/2}$. Evaluating the bias of (t_*, S_*) is an empirical matter. For a given sample, the bias will depend on the dimensionality of the data, the rate of contamination and the distance separating the outliers from the good part of the data. Finally, the bias also depends on the spatial configuration of the outliers

(the choice of \mathcal{F}_c). Fortunately, for affine equivariant algorithms the outlier configurations causing the largest biases are known and so we can focus on these cases.

3.2. Miss-classification rate. We can also compare the outlyingness indexes in terms of rate of contamination of a subset H . Denoting I_c the index set of the contaminated observations and $\mathcal{I}(\cdot)$ the indicator function, the misclassification rate is:

$$(3.3) \quad \text{Miss.Rate}(I_c, H) = \frac{\sum_{i \in H} \mathcal{I}(i \in I_c)}{\sum_{i=1}^n \mathcal{I}(i \in I_c)} .$$

This measure is always in $[0, 1]$, thus yielding results that are easier to compare across dimensions and rates of contamination. A value of 1 means that the H contains all the outliers. The main difference with the bias criterion is that the misclassification rate does not account for how disruptive the outliers are. For example, when ν is small, it is possible for $\text{Miss.Rate}(I_c, H_*)$ to be large without a commensurate increase in $\text{bias}(S_*)$. For FastPCS and SDE, using $\text{Miss.Rate}(I_c, H_*)$ also has the advantage that this criterion does not depend on the auxiliary estimate S_* since it is based on the outlyingness index directly.

3.3. Outlier configurations. We generate many contaminated datasets X_ε of size n with $X_\varepsilon = X_u \cup X_c$ where X_u and X_c are, respectively, the genuine and outlying part of the sample. The bias depends on the distance between the outliers and the genuine observations which we will measure by

$$(3.4) \quad \nu = \min_{i \in I_c} \sqrt{d_{M,i}^2(t_u, S_u) / \chi_{0.99,p}^2} .$$

The bias also depends on the spatial configuration of X_c . For affine equivariant algorithms, the worst-case configurations (those causing the largest bias) are known. In increasing order of difficulty these are:

- Shift configuration. If we constrain the adversary to (a) $|\Sigma_c| \geq |\Sigma_u|$ and (b) place X_c at a distance ν of X_u , then, to maximize the bias, the adversary will set $\Sigma_c = \Sigma_u$ (Theorem 1 in Rocke and Woodruff 1996) and set μ_c in order to satisfy (b). Intuitively, this makes the components of the mixture least distinguishable from one another.
- Point contamination. If we omit the constraint (a) above but keep (b), the adversary will place X_c in a single point so $|\Sigma_c| = 0$ (Theorem 2 in Rocke and Woodruff 1996).

- If we omit both constraints (a) and (b), the adversary may set $\mu_c = \mu_u$ and choose Σ_c to obtain a large bias. The barrow wheel contamination (Stahel and Maechler 2009) does this.

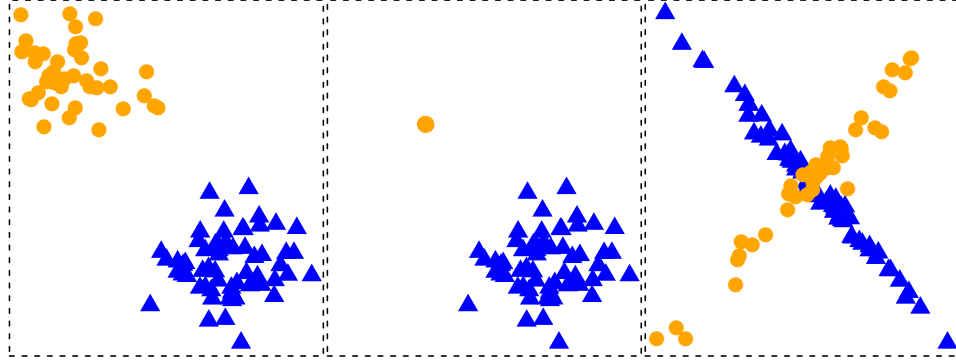


FIG 3. The three outlier configurations (Cluster, Point-Mass and Barrow Wheel). The outliers are depicted as orange dots.

We also considered other configurations such as radial outliers, but they posed little challenge for any of the algorithms, so these results are not shown.

3.4. Simulation parameters. We can generate both the uncontaminated data X_u and the contaminated data X_c from the standard normal distribution since all methods under consideration are affine equivariant. For the shift and point configurations, we will also generate data from the standard Cauchy distribution in order to quantify the sensitivity of each method to the tail index of the data.

For the shift and point configurations we generated the outliers by setting Σ_c as either D_p or $10^{-4}D_p$ (D_p denotes a rank p diagonal matrix) and $\mu_c = \eta d$ in which d is the eigenvector of S_u corresponding to its smallest eigenvalue and η is chosen to satisfy equation (3.4). We generated the barrow wheel configuration using the **robustX** package (Stahel and Maechler 2009) with default parameters. The three configuration types are depicted in Figure 3 for $n = 100$, $p = 2$, $\varepsilon = 0.4$, $\nu = 2$ and \mathcal{F}_u is the bivariate normal. The outlying observations are the orange triangles. The complete list of simulation parameters follows:

- the dimension p is one of $\{4, 8, 12, 16\}$,
- the sample size is $n = 25p$,
- the contamination fraction ε is one of $\{0.1, 0.2, 0.3, 0.4\}$,
- the configuration of the outliers is either shift, point, or barrow wheel,
- for shift and point contamination, the distance ν comes from the uniform distribution on $(0, 10)$. The barrow wheel contamination does not depend on ν .

- the number of initial $(p + 1)$ -subsets M_p is given by

$$(3.5) \quad M_p = \frac{\log(0.01)}{\log(1 - (1 - \varepsilon_0)^{p+1})}$$

with $\varepsilon_0 = 0.4$ so that the probability of getting at least one uncontaminated subset is always at least 99 percent.

In Figures 4 to 10 we display the bias and the misclassification rate (left and right plots, respectively) for discrete combinations of the dimension p , and contamination rate ε . In all cases, we expect the outlier detection problem to become monotonically harder as we increase p and ε so not much information will be lost by considering a discrete grid of a few values for these parameters. For the barrow wheel, p and ε are the only parameters we have and so we can chart the results as trellises of boxplots (Deepayan 2008).

For the shift and point contamination models, the configurations also depend on the distance separating the data from the outliers. Here, the effects of ν on the bias is harder to foresee: clearly nearby outliers will be harder to detect but misclassifying distant outliers will increase the bias more. Therefore, we will test the algorithms for many values (and chart the results as a function) of ν . For both the bias and the misclassification rates curves, for each algorithm, a solid colored line will depict the median and a dotted line (of the same color) the 75th percentile. Here, each panel will be based on 1000 simulations.

3.5. Simulation results (a). The first part of the simulation study covers the case where there is no information about the extent to which the data is contaminated. Then, we have to set h to its lower bound of slightly more than the majority of the observations.

In Figure 4 we display the bias ($\text{bias}(S_*)$) and the misclassification rate ($\text{Miss.Rate}(I_c, H_*)$) curves of each algorithm as a function of ν for different values of p and ε for the shift configuration when \mathcal{F}_u is the standard normal. All the methods perform well until $\varepsilon = 0.3$ and ≤ 8 . For larger values of p and ν , the bias curves and misclassification rate of FastMVE and SDE clearly stand out for values of ν between 2 and 6. Eventually, as we move the outliers further away, SDE and FastMVE can again find them reliably.

When \mathcal{F}_u is Cauchy (Figure 5), FastMVE performs significantly worse than the other algorithms starting already at $\varepsilon = 0.2$ and $p \geq 12$. Eventually, ($\varepsilon = 0.3$ and $p \geq 12$) FastMCD also breaks away from Σ_u . SDE performs better until $\varepsilon = 0.4$, where it is also noticeably affected by the thicker tails of

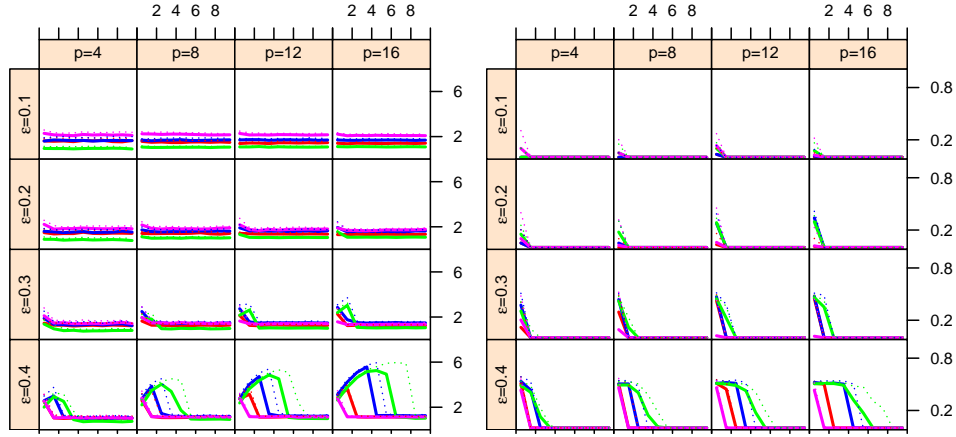


FIG 4. Bias (left) and misclassification rate (right) due to shift contamination for $\varepsilon = \{0.1, \dots, 0.4\}$, $p = \{4, \dots, 16\}$ and Normal-distributed observations shown as a function of ν . *FastMCD*, *FastMVE*, *SDE*, *FastPCS*.

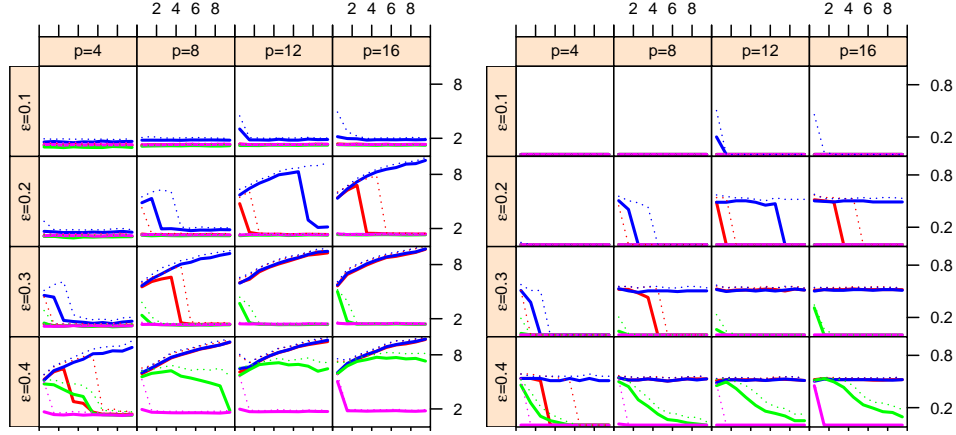


FIG 5. Bias (left) and misclassification rate (right) due to shift contamination for $\varepsilon = \{0.1, \dots, 0.4\}$, $p = \{4, \dots, 16\}$ and Cauchy-distributed observations shown as a function of ν . *FastMCD*, *FastMVE*, *SDE*, *FastPCS*.

the Cauchy distribution and fails to identify the outliers. FastPCS maintains constant and low bias (and misclassification) throughout.

In Figure 6 we show the results for the more difficult case of point-mass contamination when \mathcal{F}_u is the standard normal. Starting at $\varepsilon = 0.2$, the bias curves and misclassification rate of FastMCD becomes very high (except for $p = 4$). Starting at ($\varepsilon = 0.3$ and $p \geq 8$) all the algorithms except FastPCS fail to reliably find the outliers: looking at the misclassification rate, the optimal h -subsets for SDE, FastMVE and FastMCD even contain a higher contamination rate than ε .

The Cauchy case shown in Figure 7 is also interesting. It suggests, again, that FastMCD and FastMVE are very sensitive to fat tails in the distribution

of the good part of the data. The behavior of SDE is roughly in line with Figure 6. Again, we see that FastPCS is the only algorithm that can reliably find the outliers. Furthermore, the misclassification rates reveal that the H_* found by SDE, FastMCD and FastMVE often contains a proportion of outliers higher than the original dataset.

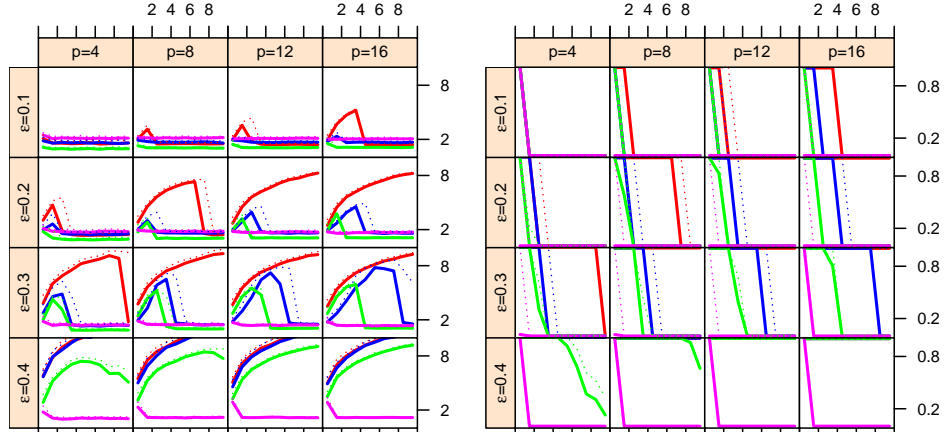


FIG 6. Bias (left) and misclassification rate (right) due to point-mass contamination for $\varepsilon = \{0.1, \dots, 0.4\}$, $p = \{4, \dots, 16\}$ and Normal-distributed observations shown as a function of ν . *FastMCD*, *FastMVE*, *SDE*, *FastPCS*.

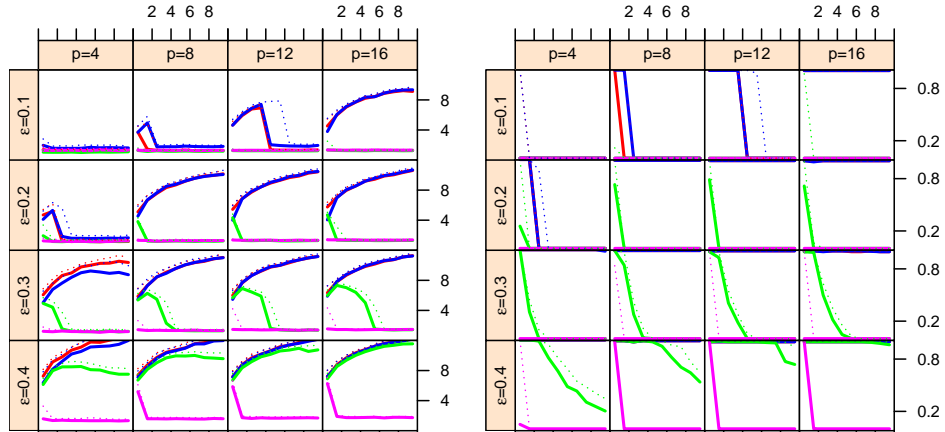


FIG 7. Bias (left) and misclassification rate (right) due to point-mass contamination for $\varepsilon = \{0.1, \dots, 0.4\}$, $p = \{4, \dots, 16\}$ and Cauchy-distributed observations shown as a function of ν . *FastMCD*, *FastMVE*, *SDE*, *FastPCS*.

In Figure 8 we show the bias curves for the barrow wheel as boxplots. FastMCD performs badly compared to the other methods, and FastMVE deteriorates for ε larger than 30 percent. It is at $\varepsilon = 0.4$ that FastPCS demonstrably exhibits superior performance, with SDE producing results in between the other three algorithms.

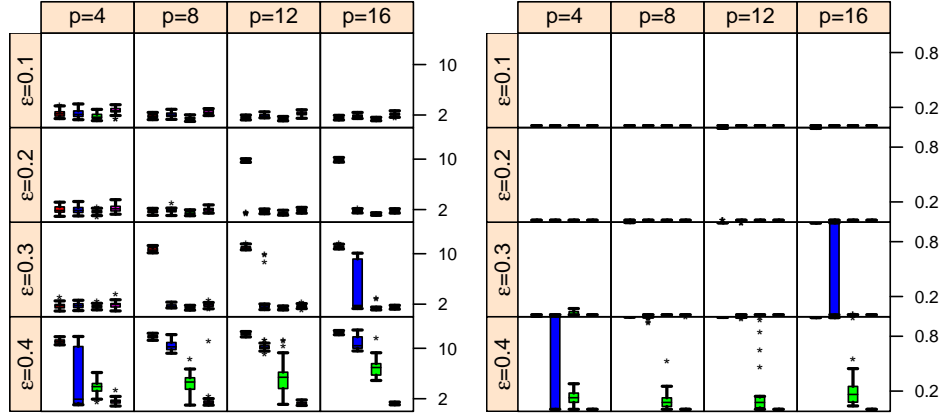


FIG 8. Bias (left) and misclassification rate (right) due to the barrow wheel contamination for $\varepsilon = \{0.1, \dots, 0.4\}$ and $p = \{4, \dots, 16\}$. *FastMCD*, *FastMVE*, *SDE*, *FastPCS*.

Across the tests, FastPCS consistently maintains low and stable biases and misclassification rates. Furthermore, the performance of FastPCS is relatively insensitive to whether ν , ε and p are low or high. Additionally, in contrast with the other algorithms, FastPCS is unaffected by the thickness of the tails of \mathcal{F}_u . The consistent ability of FastPCS to detect outliers is a highly desirable feature, which we characterize as a form of qualitative robustness.

3.6. Simulation results (b). In this section, we consider the case, important in practice, where the user can confidently place an upper bound on the rate of contamination of the sample. To fix ideas, we will set q , or the number of observations assumed to follow a model, to approximately $q = 3n/4$ (to avoid confusion we will always use h to indicate subsets of approximately $n/2$ observations). For FastPCS, FastMVE and FastMCD we adapt the algorithms by setting their respective α parameter to 0.75. SDE does not have a corresponding parameter, so we take as member of Q_* the (approximately) $3n/4$ observations with smallest outlyingness. Furthermore, we reduce the number of starting subsets (FastPCS, FastMCD, FastMVE) and random directions (SDE), by using equation (3.5), but this time setting $\varepsilon_0 = 0.2$. Then, as before, we measure the effect of our various configurations of outliers on the estimators (but this time only considering values of $\varepsilon \in \{0.1, 0.2\}$).

In Figures 9 and 10, we show the simulation results for shift and point-mass contamination. The results for Normal-distributed observations are shown in the first two rows, while the last two rows show the results for observations drawn from the multivariate Cauchy distribution. The shift contamination results in Figure 9 show that when we increase the size of the active subsets, FastPCS still maintains a low bias and misclassification

rate, but at equivalent rates of contamination, the other algorithms exhibit noticeably weaker performance than in Figures 4 and 5. Results in Figure 10 illustrate that under point-mass contamination, FastPCS again reports good results. The other algorithms continue to exhibit larger biases and misclassification rates (at equivalent rates of contamination) than in Figures 6 and 7. We do not show the results for the barrow wheel because all the algorithms perform equivalently.

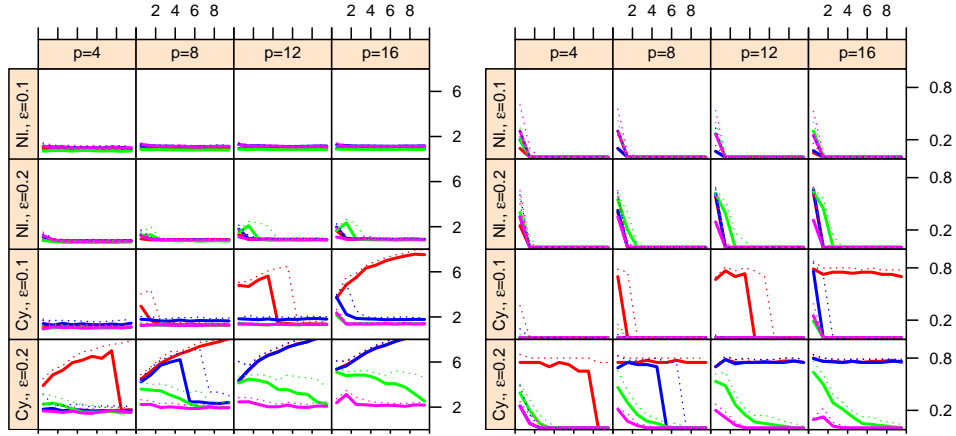


FIG 9. Bias (left) and misclassification rate (right) due to the shift contamination for $q \approx 3n/4$, $\varepsilon = \{0.1, 0.2\}$ and $p = \{4, \dots, 16\}$. The first (last) two rows are for multivariate normal (Cauchy) distributed r.v. *FastMCD*, *FastMVE*, *SDE*, *FastPCS*.

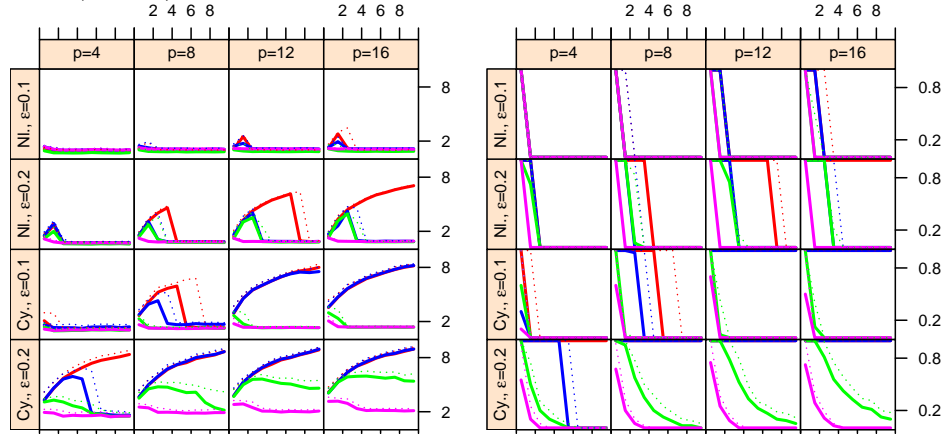


FIG 10. Bias (left) and misclassification rate (right) due to point-mass contamination for $q \approx 3n/4$, $\varepsilon = \{0.1, 0.2\}$ and $p = \{4, \dots, 16\}$. The first (last) two rows are for multivariate normal (Cauchy) distributed r.v. *FastMCD*, *FastMVE*, *SDE*, *FastPCS*.

3.7. Small Sample Accuracy. For affine equivariant outlier detection algorithms there is a trade-off between bias and accuracy (Rousseeuw 1994). This is especially problematic in small n and low ε settings because then any reduction in bias can be partially undone by losses in small sample accuracy.

For FastPCS in particular, this is visible in the first rows of Figures 4 and 8. In the misclassification plots, we see that for all algorithms the optimal subsets H_* are uncontaminated by outliers. Yet, the corresponding bias curves for FastPCS tend to be somewhat higher than for the other algorithms.

To improve accuracy in small samples without conceding too much in bias, a solution is to add a so-called re-weighting step to the outlier detection algorithm. In essence, we replace H_* by a larger subset J_+ , itself derived from H_* . The motivation is that, typically, J_+ will include a greater share of the uncontaminated observations. Over the years, many such re-weighting procedures have been proposed (Maronna, Martin and Yohai 2006). Perhaps the simplest is the so called hard-thresholding re-weighting. Given an optimal subset H_* , the members of J_+ are:

$$(3.6) \quad J_+ = \left\{ i : d_{M,i}^2(t_*, S_*) \chi_{0.5,p}^2 \leq d_{M,[h/n]}^2(t_*, S_*) \chi_{0.975,p}^2 \right\}.$$

Contrary to H_* , the size of J_+ is not fixed in advance. This makes it difficult to compare algorithms on the basis of $\text{bias}(S_+)$ or $\text{Miss.Rate}(I_c, J_+)$ evaluated at contaminated sub-samples X_ε . Nonetheless, we can still compare them in terms of the bias of S_+ computed at uncontaminated data sets X_u and for various sample sizes n . In essence, we measure the finite sample accuracy of the various algorithms by considering their biases at uncontaminated datasets as a function of n . In Figure 11, we show the results of doing this for $n = \{100, 200, \dots, 500, 599\}$ (shown as the abscissa) and $p = 8$. We set 599 observations as an upper limit because when $n \geq 600$ FastMCD uses a nested sub-sampling scheme whereby larger datasets are divided unto non overlapping sub-samples of at most 600 observations.

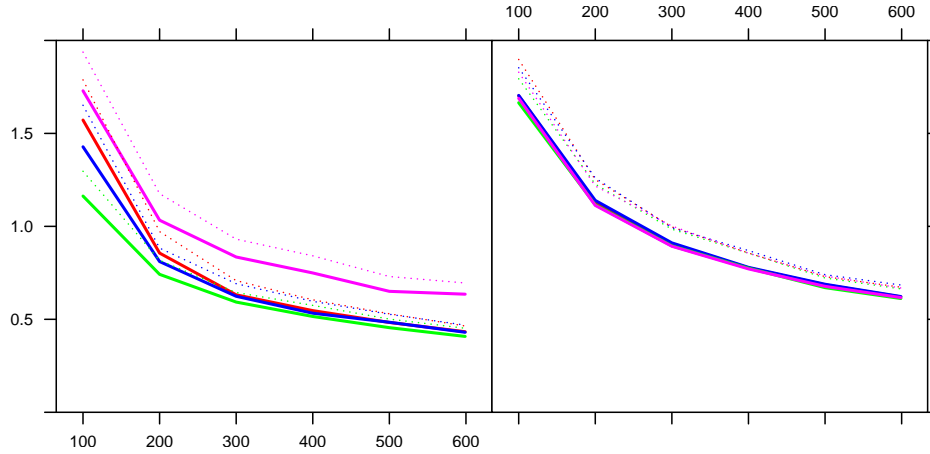


FIG 11. Empirical bias at uncontaminated samples for $p = 8$ as a function of sample size. *FastMCD*, *FastMVE*, *SDE*, *FastPCS*.

Figure 11 depicts the median (solid) and 75th percentile (dotted) accuracy

curves of the algorithms for increasing n when \mathcal{F}_u is normally distributed (left) and Cauchy distributed (right). Each panel is based on 1,000 experiments. As expected, FastPCS is noticeably less accurate than the other algorithms in the Gaussian case. Nonetheless, we maintain that this difference is small compared to the reduction in bias achieved by FastPCS on contaminated samples. Furthermore, this gap in performance depends on the distribution of the good data: when \mathcal{F}_u is Cauchy the accuracy of FastPCS is similar to that of the other algorithms.

4. Empirical Comparison: Case Study. In this section, we illustrate the behavior of FastPCS on a real data problem from the field of engineering: the Concrete Slump Test Data set (Yeh 2007). This dataset includes 103 data-points, each corresponding to a different type of concrete. For each observation we have 7 so-called input variables measuring, respectively, the quantity of cement (kg/m³), fly ash (kg/m³), blast furnace slag (kg/m³), water (kg/m³), super-plasticizer (kg/m³), coarse aggregate (kg/m³), and fine aggregate (kg/m³) used to make the corresponding variety of concrete. Additionally, for each observation, we have 3 so-called output variables measuring attributes of the resulting concrete. These are slump (cm), flow (cm) and 28-day compressive strength (Mpa).

This dataset actually contains two groups of observations collected over separate periods. The first 78 measurements pre-date the last 25 by several years. An interesting aspect of this dataset is that these two groups largely overlap on bivariate scatter-plots of the data, forming a seemingly homogeneous group of observations. Appearances can be deceptive and when considered along all variables jointly however, the two groups are clearly distinct. For example, denoting J_O (J_N) the subset of 78 (25) members of the early (latter) batch of measurements, we find that the closest member of J_N lies at a squared Mahalanobis distance of over 760 with respect to (t_O, S_O) . As a point of comparison, this is nearly 32 times larger than $\chi^2_{0.99,10}$.

We first ran the SDE, FastMCD, FastMVE and FastPCS algorithms on the raw dataset (for the first three, we used the `rrcov` implementations with default parameters). We set the number of random directions in SDE and the number of random p -subsets in FastMCD, FastMVE and FastPCS to $M_p = 2000$, as given in equation (3.5). To have comparable results, we will use for each estimator $d_{M,i}(t_*, S_*)$, the vector of statistical distances wrt H_* .

The Mahalanobis outlyingness indexes are displayed in the first column of Figure 12, Concrete (i). Each row corresponds to an estimator. For each estimator we drew two boxplots. The first one (blue) depicts the outlyingness index for the 78 members of J_O and the second (orange) boxplot for those

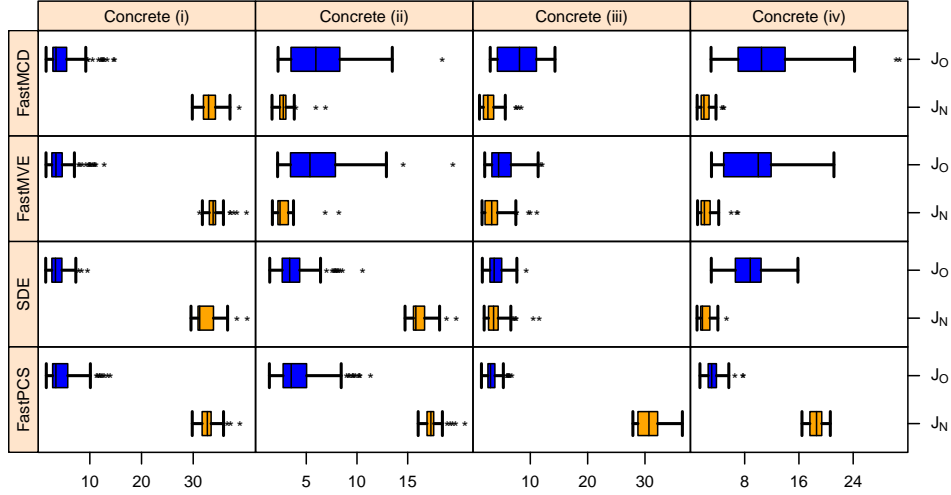


FIG 12. Mahalanobis outlyingness index $d_{M,i}(t_*, S_*)$ for the four estimators and the four variants of the concrete dataset. In each panel, the blue (orange) boxplot depicts $d_{M,i}(t_*, S_*)$ for the members of J_O (J_N).

25 members of J_N . All the algorithms are able to unambiguously separate the two subgroups of observations: the outlyingness values assigned to the members of the more recent batch of observations are notably larger than the outlyingness values assigned to any members of J_O .

In a second experiment, Concrete(ii), we made the original outlier detection problem harder by narrowing the distance separating the outliers from the genuine observations. To do so, we pulled the 25 outliers towards the mean of the good part of the data by replacing the original outliers with 25 observations of the form $x_{n+i}^{ii} \leftarrow (x_{n+i} + t_O)/2$ for $1 \leq i \leq 25$, $n = 78$. We denote J_N^{ii} to be these 25 members of $x_{n+i} | 1 \leq i \leq 25$. The second column of Figure 12 depicts the outlyingness indexes for this second experiment. Again, for each algorithm, the first (blue) boxplots depict the values of the outlyingness indexes for the 78 members of J_O and the second (orange) boxplot for the 25 members of J_N^{ii} . Note that the members of J_N^{ii} still form a cluster that is genuinely separate from the main group of observations. For example, the closest member of J_N^{ii} lies at a squared Mahalanobis distance of over 190 with respect to (t_O, S_O) . For comparison, this is over 8 times larger than $\chi_{0.99,10}^2$. Here, the FastPCS and SDE outlyingness indexes continue to clearly distinguish between the two groups. The outlyingness indexes derived from FastMVE and FastMCD however fail to adequately flag the outliers. These results are consistent with those of the synthetic data experiments where we found that the performance of these algorithms are overly sensitive to the distance separating the outliers from the data.

In a third experiment, Concrete(iii), we made the original outlier de-

tection problem harder still by increasing the contamination rate of the sample. This was done by adding an additional 25 outliers of the form $x_{n+k}^{iii} \leftarrow (x_{n+i} + x_{n+j})/2$ for $1 \leq i, j, k \leq 25$, $n = 78$. We denote J_N^{iii} the members of this third set of 50 outliers. The third column of Figure 12 depicts the outlyingness indexes for this experiment. Again for each algorithm, a blue boxplot pertains to the 78 members of J_O and an orange one to the 50 members of J_N^{iii} . For SDE, FastMVE and FastMCD we can see that increasing the contamination rate of the sample causes the outlyingness indexes of the two groups to overlap while the outlyingness index produced by FastPCS continues to make a clear distinction. Remarkably, the subsets of h observations with the smallest outlyingness chosen by the first three algorithms are primarily composed of outliers.

In a final experiment, Concrete(iv), we narrowed the distance between the good data and the outliers (as in Concrete(ii)), and increased the contamination rate (as in Concrete(iii)). The fourth column of Figure 12 depicts the outlyingness indexes for this experiment, again with for each algorithm a blue boxplot for the 78 members of J_O and an orange for the 50 members of J_N^{iv} . Here again, the outlyingness index of SDE, FastMCD and FastMVE fails to adequately flag the outliers. However, as with each of the previous experiments, FastPCS still assigns a larger index of outlyingness to the members of the outlying group.

Overall, we see that the results of the real data experiment confirm those of the simulations, at least qualitatively. When the contamination rates are small and the outliers well separated from the good part of the data, all outlier detection methods seem to perform equally well. As we consider more difficult outlier settings however, we see that the FastPCS outlyingness index is the only one that identifies the outliers reliably.

5. Outlook. In this article we introduced PCS, a new outlyingness index and FastPCS, a fast and affine equivariant algorithm for computing it. Like many other outlier detection algorithms, the performance of FastPCS hinges crucially on correctly identifying an h -subset of uncontaminated observations. Our main contribution is to characterize this h -subset using a new measure of congruence of a multivariate cloud of points. This new characterization was designed to be insensitive to the configuration of the outliers.

In our simulations, we have focused on configurations of outliers that are worst-case for affine-equivariant algorithms and found that FastPCS behaves notably better than the other procedures we considered, often revealing outliers that would not have been identified by the other approaches. In practice, admittedly, contamination patterns will not always be as difficult as those

we considered above and in many cases the different methods will, hopefully, mostly concur. Nevertheless, given that in practice we do not know the configuration of the outliers, as data analysts, we prefer to carry our inferences while planing for the worst contingencies.

Also through simulations, we found that the performance of FastPCS is not affected much by the tail index of the majority of the data. For example, FastPCS is capable of finding the outliers both when the majority of the data is distributed multivariate normal, or is drawn from a heavy-tailed distribution, such as the multivariate Cauchy.

In this article we emphasized the practical aspects of PCS. A number of theoretical properties deserve further investigation. In particular, we suspect that PCS has maximum breakdown point. Arguments supporting this conjecture are that the maximum biases are low and that the procedure has the exact fit property.

References.

- [1] Deepayan, S. (2008). *Lattice: Multivariate Data Visualization with R*. Springer.
- [2] Maronna R. A., Martin R. D. and Yohai V. J. (2006). *Robust Statistics: Theory and Methods*. Wiley, New York.
- [3] R Core Team (2012). *R: A Language and Environment for Statistical Computing*. R Foundation for Statistical Computing. Vienna, Austria.
- [4] Rocke D. M. and Woodruff D. L. (1996). Identification of Outliers in Multivariate Data. *Journal of the American Statistical Association*, 91, 1047–1061.
- [5] Rousseeuw, P. J. and van Zomeren B.C. (1990). Unmasking Multivariate Outliers and Leverage Points. *Journal of the American Statistical Association* , Vol. 85, No. 411, pp. 633-639
- [6] Rousseeuw, P. J. (1994). Unconventional features of positive-breakdown estimators. *Statistics and Probability Letters*, 19, 417–431.
- [7] Rousseeuw P. J. and Van Driessen K. (1999). A Fast Algorithm for the Minimum Covariance Determinant Estimator. *Technometrics*, 41, 212–223.
- [8] Stahel W. (1981). Breakdown of Covariance Estimators. Research Report 31, Fachgrupp für Statistik, E.T.H. Zürich.
- [9] Stahel W. and Maechler M. (2009). *robustX: eXperimental eXtraneous eXtraordinary ... Functionality for Robust Statistics*. R package version 1.1-2.
- [10] Todorov V. and Filzmoser P. (2009). An Object-Oriented Framework for Robust Multivariate Analysis. *Journal of Statistical Software*, 32, 1–47.
- [11] Yeh, I. (2007). Modeling slump flow of concrete using second-order regressions and artificial neural networks. *Cement and Concrete Composites*, Vol.29, No. 6, 474–480.
- [12] Yohai, V.J. and Maronna, R.A. (1990). The Maximum Bias of Robust Covariances. *Communications in Statistics–Theory and Methods*, 19, 3925–2933.

STATISTICS SECTION, DEPARTMENT OF MATHEMATICS
 CELESTIJNENLAAN 200B - BOX 2400
 3001 HEVERLEE
 E-MAIL: kaveh.vakili@wis.kuleuven.be
 eric.schmitt@wis.kuleuven.be
 URL: <http://wis.kuleuven.be/stat/robust>